Aggressive Neuroblastomas Start Growing after Infancy

Daniel L. Monyak,[1] Shannon T. Holloway,[2] Graham J. Gumbert,[1] Kellie Kim,[3] Allison Fong,[3] Lars J. Grimm,[4] Jeffrey R. Marks,[5] Marc D. Ryser,[2,6]* Darryl Shibata[3]*

Affiliations

[1]Trinity College of Arts and Sciences, Duke University; Durham, NC, USA.

[2]Department of Population Health Sciences, Duke University School of Medicine; Durham, NC, USA.

[3]Department of Pathology, University of Southern California Keck School of Medicine; Los Angeles, CA, USA.

[4]Department of Radiology, Duke University School of Medicine; Durham, NC, USA.

[5]Department of Surgery, Duke University School of Medicine; Durham, NC, USA.

[6]Faculty of Medicine, University of Geneva; Geneva, Switzerland.

*Corresponding authors. marc.ryser@unige.ch; dshibata@usc.edu

Abstract

In neuroblastoma, population screening during infancy failed to lower mortality because it primarily detected biologically indolent tumors rather than aggressive, life-threatening disease. The failure may reflect limited screening sensitivity, or disease onset after infancy among aggressive tumors. Here, we used an epigenetic mitotic clock based on fluctuating CpG DNA methylation to estimate patient-specific tumor mitotic ages and calendar ages in a cohort of unscreened children diagnosed with neuroblastoma. Aggressive cancers (stage 4) primarily started growing after the first year of life, making them undetectable by screening during infancy. In contrast, biologically indolent tumors (stages 1, 2, 3 and 4S) often started growing in utero or during the first year of life, and affected children had better survival outcomes. Due to a short preclinical detectable phase of aggressive neuroblastomas, reducing mortality through screening is impractical as it would require frequent screening among older children. Patient-specific tumor-age estimation may help refine screening windows and improve early-detection strategies in other cancers where screening has so far failed to yield substantial mortality reduction.

INTRODUCTION

Early detection is a cornerstone of cancer control, aiming to identify tumors before clinical symptoms emerge—when they are smaller, less invasive, and more likely to be curable. The effectiveness of this approach depends on the tumor's sojourn time—the interval during which a malignant lesion is screen-detectable but asymptomatic (1). Screening tests preferentially uncover slow-growing tumors with long sojourn times; rapidly growing tumors are more difficult to intercept because their sojourn times are often short compared to the screening interval. Due to this length bias (2), screening can only incur a mortality reduction if the sojourn times of aggressive cancers are sufficiently long for effective interception. If this is not the case, screening instead leads to overdiagnosis and overtreatment in the absence of a mortality benefit (3).

In the case of neuroblastoma (NB), a common pediatric cancer, substantial efforts were made in the 1990s to develop a urine-based early detection test screening for cancer metabolites (4). While screening successfully identified small, asymptomatic tumors, its utility was limited by the fact that many NBs are biologically indolent or even spontaneously regress without treatment (5, 6). Screening during the first year of life primarily detected good-outcome tumors rather than aggressive NBs. In consequence, large-scale early efforts to screen for NBs in infants conclusively failed to reduce mortality and NB screening was abandoned (4, 7-9).

Neuroblastomas can begin to grow before birth (10, 11), and mutations found in tumors at the time of removal have been inferred to occur as early as the first trimester (12, 13). The failure of screening suggests two possibilities: either the test did not manage to detect asymptomatic aggressive tumors during the first year of life, or these aggressive tumors simply had not yet begun to grow during infancy **(Figure 1A**). To identify the more likely reason of failure, we developed an epigenetic clock to determine tumor age based on fluctuating CpG (fCpG) DNA methylation (**Figure 1B**) (14, 15). Using this clock, we estimated the mitotic ages of individual tumors—that is the number of cell doublings between the most common recent ancestor cell and the resected specimen—in an unscreened cohort of NB patients. We found that aggressive NBs were mitotically younger than indolent ones and primarily started growing after the first year of life. Short sojourn times rather than low test sensitivity is thus most likely what undermined the effectiveness of NB screening during infancy (**Figure 1A**).

RESULTS

Estimating Tumor Mitotic Age in Neuroblastoma Patients

A neuroblastoma fCpG clock was constructed as previously described (15). In brief, we analyzed methylation data (850K EPIC array) from 213 tumors from the neuroblastoma TARGET cohort (16) to identify a set of 1,000 fluctuating CpG sites whose average methylation values (β-values, between 0 and 1) were balanced (mean ~0.5) and dispersed (large inter-tumor variance).

At the start of growth of the tumor, fCpG methylation in the most recent common ancestor cell can only be 0, 0.5, or 1. As the tumor mass grows, the average methylation at fCpG sites that were originally unmethylated ($\beta = 0$) or fully methylated ($\beta = 1$) will slowly drift to $\beta = 0.5$. Therefore, by measuring the methylation distribution in an ensemble of fCpGs, we can distinguish younger tumors with discrete peaks in the methylation distribution (low epigenetic entropy) from older tumors with a unimodal distributions centered around $\beta = 0.5$ (high epigenetic entropy; **Figure 1C**). To produce a quantitative estimate of tumor mitotic age, we inferred the location of the left and right peaks in the histograms (**Figure 1C**) and converted peak location to mitotic age based on a simple mathematical model of the stochastic oscillator at each fCpG site; see **Methods** for details.

Aggressive NBs Expand after Infancy

The conversion from tumor mitotic to calendar age requires calibration of the molecular clock. In adult malignancies, the unobservable start of expansion from a single progenitor cell can predate the date of diagnosis by decades, rendering direct calibration impractical. In pediatric cancers, however, the calendar age of tumors is much more constrained because the start of growth cannot predate conception. Noting that NBs can be found as early as the first trimester (10, 11), we used patients who were diagnosed shortly after birth to convert tumor mitotic age (cell doublings) into tumor calendar ages (years); see **Methods** for details.

As visualized in **Figure 2**, most NBs diagnosed during infancy (first year of life) started growth prenatally or shortly after birth. In 166/167 (99.4%) of cancers diagnosed after 1.5 years of patient age, tumor growth started after the first year of age, that is after the typical screening period for NB. Overall, 163 of 167 stage 4 NBs (97.6%) started to grow after one year of age, whereas 42 of 46 (91.3%) of more indolent NBs (stages 1,2,3,4S) started to grow before one year of age.

Our tumor age estimate includes the initial expansion phase when the growing mass is too small to be screen detectable. Nevertheless, it provides an upper bound to the sojourn time—the period when the tumor is asymptomatic but screen-detectable. Based on our analysis, the mean sojourn time among aggressive stage 4 tumors was 109 days (range, 29 to 329 days) compared to 126 days (range, 46-262 days) among indolent (stages 1,2,3,4s) tumors (P = 0.03; two-sided t-test).

In summary, in this cohort, even the most sensitive screening test would have failed to detect a clinically significant proportion of lethal NBs during infancy. These findings suggest that the historical failure of NB screening to reduce mortality (4, 9) was likely due to the fact that aggressive tumors only initiate after end of the screening window.

Tumor Mitotic Age Correlates with Prognostic Factors

Among unscreened patients, NB usually presents as a palpable mass. By the time they reach a macroscopic size, slow-growing tumors are expected to have accumulated more cell divisions and appear mitotically older compared to fast-growing and aggressive NBs. We tested this hypothesis by investigating the relationship between tumor mitotic age and prognostic factors in a cohort of unscreened NB cases.

As predicted, stage 1 and 4S tumors were mitotically older compared to metastatic stage 4 cancers (**Figure 3A**). Similarly, tumors classified as high-risk were mitotically younger tumors compared to low-risk tumors (**Figure 3B**). Tumors with MYCN amplification (a marker of aggressiveness) were mitotically younger than tumors without MYCN amplification (**Figure 3C**), and patients diagnosed before the age of 1.5 had mitotically older tumors (**Figure 3D**). We validated these finding in a second cohort of 105 clinically detected NB tumors (17).

Finally, for a more systematic analysis, we leveraged the availability of gene expression (RNA-seq) data in the TARGET cohort to perform a gene-set enrichment analysis (GSEA). Mitotically younger NBs were enriched for proliferation pathways; no pathway enrichment was identified for older NBs.

Tumor Age Predicts Survival

Extending our analysis beyond prognostic factors, we examined the relationship between tumor mitotic age and cancer-related mortality. Indeed, because pediatric cancer patients have a low risk of death from cancer-

unrelated causes, overall survival provides a good proxy for disease-specific survival. In a univariate Cox model, younger tumor mitotic age was associated with lower overall survival (HR 0.16; 95% CI, 0.046-0.55; P = 0.004; **Figure 4A**). Even after adjusting for clinical risk group, younger mitotic age remained an independent predictor of poor survival (HR 0.26; 95% CI, 0.079-0.84; P = 0.025; **Figure 4B**).

DISCUSSION

Neuroblastoma screening increased the incidence of biologically favorable tumors without reducing the incidence of lethal cancers and mortality (4, 9). What remains unclear, however, is why lethal cancers were missed in the first place: was the test's sensitivity to detect aggressive phenotypes too low, or did these tumors only start growing after the screening period? Applying an epigenetic molecular clock to a cohort of unscreened neuroblastoma patients, we show that most aggressive stage 4 tumors started growing after the first year of life. As such they were not present—and thus not detectable—during infancy. In contrast, most tumors with a more favorable biology started growing before or shortly after birth (12), rendering them a priori screen-detectable during infancy. Our findings suggest that the failure of neuroblastoma screening was due to a mismatch between screening window and onset of lethal disease, rather than insufficient sensitivity of the test.

A second question is whether extending screening beyond the first year of life could provide a way to improve outcomes. In our analysis, we estimated the sojourn times of stage 4 cancers to be very short, of the order of a few months only, suggesting a very limited opportunity for early detection even under very frequent screening after infancy.

An increase in the incidence of favorable tumors in screened populations is a common occurrence in cancer screening and has been documented, e.g., in cancers of the breast, thyroid, prostate and lung. However, for these cancer types, the overdiagnosis of good-outcome cancers is accompanied by the detection of a proportion of aggressive cancers which in turn produces a mortality benefit of the screening test. The situation in neuroblastoma screening is different in that there the incidence of lethal cancers remained unchanged, resulting in very high rates of overdiagnosis in the absence of any screening benefit.

Methylation-based molecular clocks were originally introduced to measure biological tissue aging (18-21), and have been successfully applied to quantifying cancer risk (22, 23). A common feature of many of these clocks is that they leverage a unidirectional drift in methylation of a tissue over time. Our clock differs in that it starts—or is reset—at the onset of tumor growth, based on the fCpG methylation pattern in the final progenitor cell. This reset, along with rapid, balanced methylation and demethylation at fCpG sites, allows us to rank cancers by their

mitotic age, which may vary by only a few months. Calibrating a cancer clock—that is converting mitotic to calendar age—is challenging because the calendar ages of tumors are invariably unknown. In the case of pediatric cancers like NB, however, the natural age constraint by the date of conception provides an opportunity for calibration. The type of molecular clock we adapted here to the NB setting had previously been used to study stem cell turnover in normal human tissues (14), to show that acute leukemias exhibit synchronized "W-shaped" fCpG distributions, while chronic leukemias display desynchronized, unimodal distributions (14), and to characterize the temporal landscape of human breast cancer (15). Like for NBs, breast cancer mitotic ages vary, with more aggressive tumors tending to be mitotically younger.

Our study has several limitations. Although NB mitotic ages align well with established NB biology, a limitation of this analysis is its inferential nature. While conception provides a boundary for the maximum possible mitotic age of NBs, the calibration used for infancy may not be applicable to older children if methylation fluctuation rates change as a function of the child's age. Additionally, the clock only measures the age of the final clonal expansion; precursor progenitor cells present before the start of growth, inferred from copy number alterations and mutations (12, 13), would not be detectable by this approach (however, they wouldn't be detectable by screening either). Further refinement of the fCpG site selection and additional characterization could improve the accuracy of the clock.

Cancer early detection efforts crucially depend on organ-specific natural history of disease. To date, these dynamics have primarily been characterized by summary statistics such as the mean sojourn time, obtained by fitting mathematical models to screening and diagnosis data. The approach used in this work provides an opportunity to move from statistical averages to tumor-specific mitotic ages and sojourn times. And being based on readily available methylation array data, the molecular clock we used in this work can easily be generalized to estimate tumor-specific mitotic ages and sojourn times across various cancer types.

Acknowledgments

This work was partially supported by grant R01-CA271237 from the National Institutes of Health.

METHODS

Samples. Of the 842 neuroblastomas from patients in the Therapeutically Applicable Research to Generate Effective Treatments (TARGET) program (16), 213 had available methylation array data (Infinium HumanMethylation450 BeadChip, Illumina, San Diego, CA, USA), which were used to select an ensemble of 1000 fCpG sites. Only a single measurement was used when a tumor had 2 measurements. The following variables were retrieved: patient age at diagnosis, INSS stage, Children's Oncology Group (COG) risk group, and MYCN amplification status. Among the 213 tumors, gene expression quantification (RNA-seq) data was available for 132. All clinical and sequencing data were retrieved from the Genomic Data Commons (GDC; https://gdc.cancer.gov) using the R package *TCGAbiolinks* (version 2.25.3).

We also retrieved publicly available methylation array data (Infinium HumanMethylation450 BeadChip) from 105 neuroblastomas (17) from patients enrolled in the German Neuroblastoma Trial (GSE73515). The following variables were retrieved: patient age group at diagnosis; INSS stage; risk category, MYCN amplification status.

Selection of fluctuating CpG (fCpG) sites. First, we sought to identify CpG sites with balanced methylation and de-methylation rates, defined as having an average methylation content (β-value) between 0.4 and 0.6 in the TARGET cohort (N = 213). CpG sites with ≥20 missing values in the TARGET cohort were excluded from this selection process. In the second step, we eliminated age-confounded sites by calculating the Spearman correlation ρ between patient age at diagnosis and CpG β-value, and eliminating sites with $\rho > 0.2$. In the third step, the remaining CpG sites were ranked by their β-value variance among tumors and we eliminated the 25% least variable sites. In the final step, we aimed to select sites that had good evidence for both randomness in initial value at the birth of a tumor and no bias for being methylated or demethylated. A detailed explanation is provided in **Supplementary Methods**, but in summary, K-Means clustering was performed on the remaining CpG sites, and we defined the clock set $\mathcal{C}$ as the 1000 sites least important for cluster definition.

Pathway enrichment analyses. For the TARGET cohort, we performed a gene set enrichment analysis (GSEA) using the software package *GSEA (24)* to identify *Hallmark* gene sets that are correlated with the mitotic age ϕ. The analysis was performed using the Pearson correlation to rank individual genes; phenotype-permutation-

183 based *P* values and false-discovery rate (FDR) *Q* values were computed using 1,000 permutations. All other
184 inputs were kept at their defaults.

185 **Statistical analyses**. Correlations between two continuous variables were calculated using the Pearson
186 correlation coefficient. The medians of continuous variables were compared using a two-sided Wilcoxon rank-
187 sum test at significance level of 0.05. For each variable, tumors with missing values of that variable were
188 excluded. All analyses and visualizations were performed in Python (3.9.19) and R (version 4.3).

189 **Gaussian mixture model.** To estimate tumor mitotic and calendar ages from the empirical β-value distributions,
190 we proceeded in two steps. In the first step, we decomposed each tumor's empirical β-value distribution into
191 three peaks of fCpG sites: the originally unmethylated fCpG sites (left peak), the originally hemi-methylated fCpG
192 sites (middle peak), and the originally methylated fCpG sites (right peak). Each tumor's β-value distribution was
193 modeled as a mixture of three normal distributions: a left component centered at a free parameter X, a middle
194 component centered at 0.5, and a right component centered at $1 - X$ (see **Supplementary Methods** for more
195 detail). The variance of each component was determined by a shared effective allele number n such that the
196 variances were proportional to $X(1 - X) / n$, where X is the mean of the corresponding component. A Dirichlet
197 prior with concentration $\begin{pmatrix} 5 \\ 10 \\ 5 \end{pmatrix}$ was used on the component proportions to reflect the biological expectation of the
198 proportions of starting states of the fCpG sites being roughly 25% fully unmethylated, 50% hemi-methylated, and
199 25% fully methylated (the steady state of an fCpG in the parent cell population of the founding tumor cell). We
200 also placed a $beta(1, 4)$ prior on X to reflect the theoretical impossibility that $X > 0.5$ and a $gamma(2, 0.1)$ prior
201 on n to allow flexibility in the effective allele number.

202 **Likelihood and prior functions.** We consider a latent parameter h_i that signifies the initial state of fCpG i,
203 such that:

204 $h_i = 1 \leftrightarrows$ Site i was initially completely un-methylated

205 $h_i = 2 \leftrightarrows$ Site i was initially hemi-methylated

206 $h_i = 3 \leftrightarrows$ Site i was initially completely methylated

207 Conditional likelihood (see **Supplementary Methods**):

$\mu_1 = X$

$\mu_2 = 0.5$

$\mu_3 = 1 - X$

$\sigma^2_{h_i} = \mu_{h_i}(1 - \mu_{h_i})/n$

$Y_i \mid h_i \sim N(\mu_{h_i}, \sigma^2_{h_i})$

To avoid modeling the discrete latent parameter h_i, we use a marginal likelihood:

$$f(Y_i) = \sum_{h_i=1}^{3} p(h_i) \times p(Y_i|h_i)$$

Priors:

$h_i \sim Dir(\begin{pmatrix} 5 \\ 10 \\ 5 \end{pmatrix})$

$X \sim beta(1, 4)$

$n \sim gamma(2, 0.1)$

Bayesian inference. The above model was implemented in Stan using the R package *rstan* (version 2.36.0.9000). Sampling was performed independently for each tumor's 1000 Clock fCpG β-values for each tumor in the discovery and validation cohorts, with four chains of 4000 iterations each (2000 warmup). Excellent convergence was achieved, as assessed by inspection of chain mixing, R-hat statistics, and effective sample sizes (all parameters had an $\hat{R} < 1.02$ across all tumors in both cohorts).

Tumor age estimation. Tumor mitotic age ϕ was sampled as well, by substituting each MCMC sample of the X parameter into an equation that relates ϕ to the peak location X, based on a simple oscillatory model of fCpG evolution (see **Supplementary Methods**), and the sampling mean of ϕ for each tumor was used as tumor mitotic age throughout all further analysis. In the discovery cohort, we converted the unitless ϕ_i to calendar age t_i in days using the fact that $\phi_i = t_i \alpha_i \mu$, where α_i is the proliferation rate and μ is the constant (de-)methylation rate, and assumed a constant proliferation rate $\alpha_i = \alpha$. We then chose a value of $\alpha\mu$ such that the minimum tumor initiation time (patient age - tumor calendar age) was estimated to be 180 days, as NBs can be detected as early as the first trimester (12, 13).

232 **FIGURES**

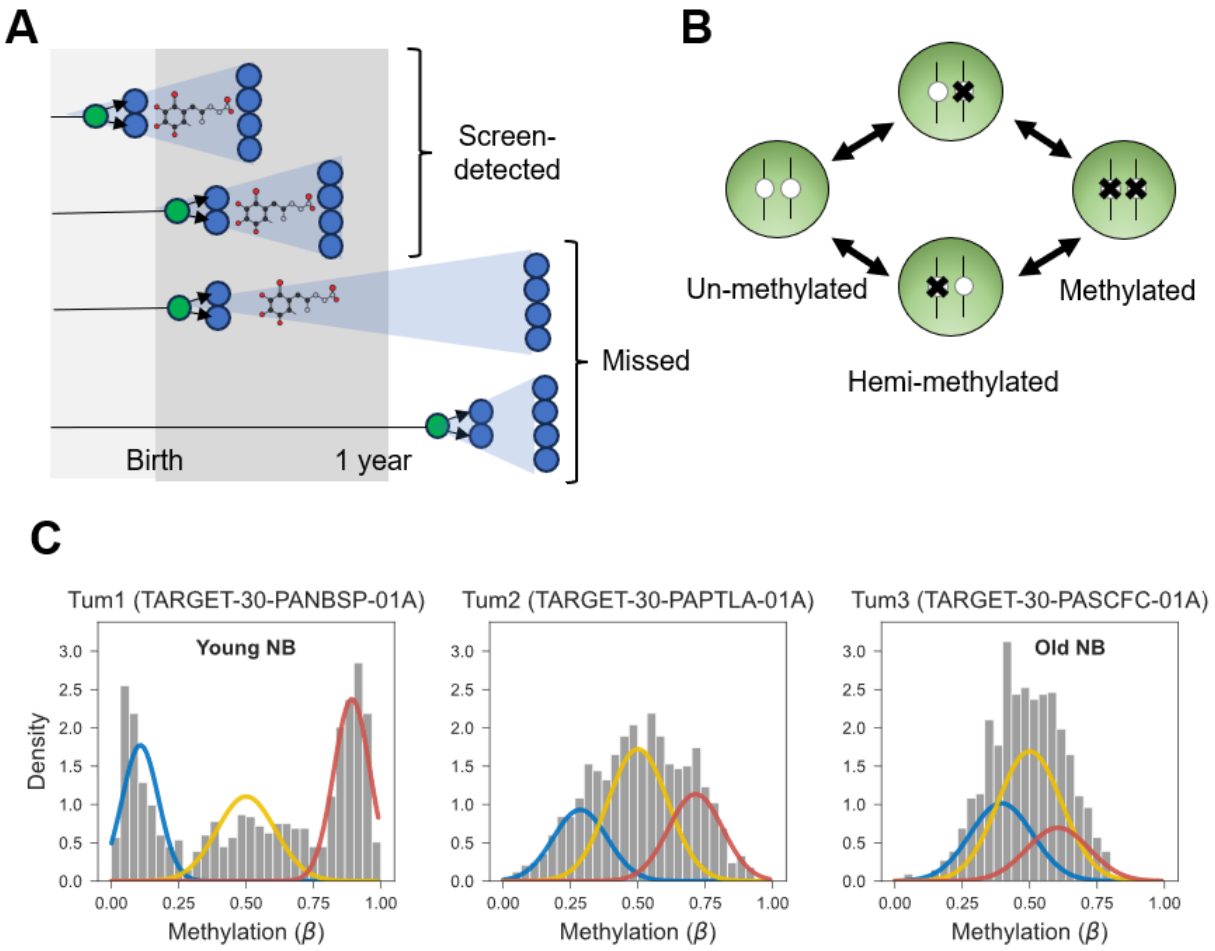

233

234 **Figure 1. Fluctuating CpG sites (fCpG) and modulators of tumor age**. **(A)** NB screening during the first year
235 of life can detect tumors that are growing during this time. NBs removed during the first year of life tend to regress
236 spontaneously and could start to grow before birth. NBs removed after the first year of life tend to progress and
237 could be growing during the first year of life (screen detectable by measuring urinary catecholamines) or could
238 start to grow after the first year of life (screen undetectable). The fCpG clock indicates that most NBs that
239 progress have short sojourn times and are not growing before the age of one year, consistent with the failure of
240 infant screening to reduce NB mortality. **(B)** fCpGs stochastically oscillate between the unmethylated, hemi-
241 methylated, and methylated states. **(C)** Examples of fCpG methylation distributions for young, middle aged, and
242 older NBs. The curves represent the inferred distributions for fCpG sites that started at 0, 50 or 100% methylation
243 in the progenitor cell. fCpG sites that start at 0 or 100% methylation progressively drift towards 50% with
244 increasing mitotic age from random but balanced methylation and demethylation. Hence, a younger NB has a
245 broader fCpG distribution whereas an older NB has a more narrow or unimodal fCpG distribution.

246

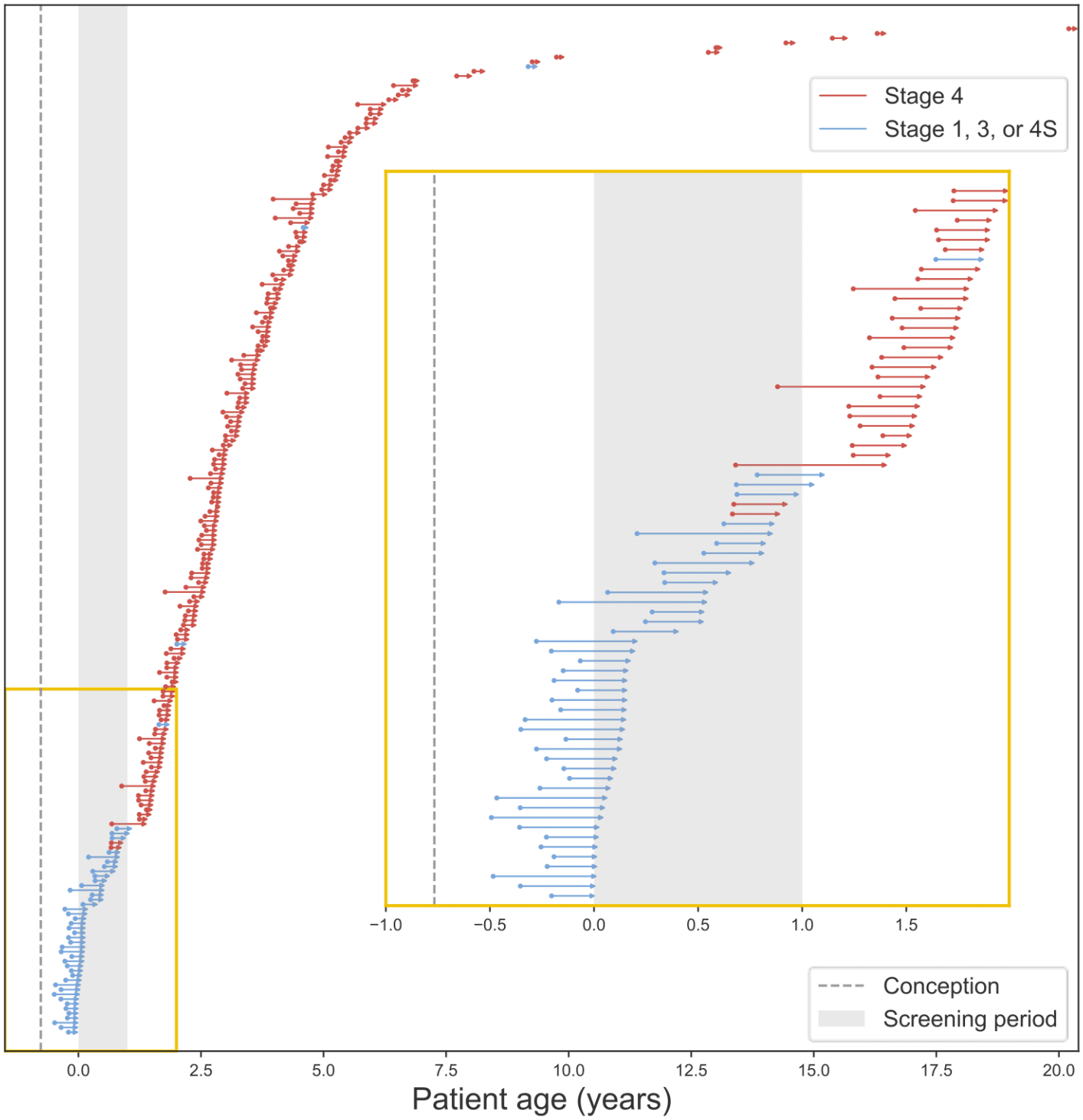

Figure 2. Inferred TARGET NB sojourn intervals. Lines connect ages at removal with their inferred ages at growth initiation. NBs are potentially screen detectable during their growth phases. Many NBs that regress start to grow before birth (but not before conception), have relatively long sojourn intervals, and are screen detectable during infancy. Most NBs that progress (Stage 4) have shorter sojourn intervals, start to grow after 1 year of age, and therefore are not screen detectable during infancy. Gray region spans first year of life. Insert: magnified view of tumors discovered in patients diagnosed before 2.5 years of age.

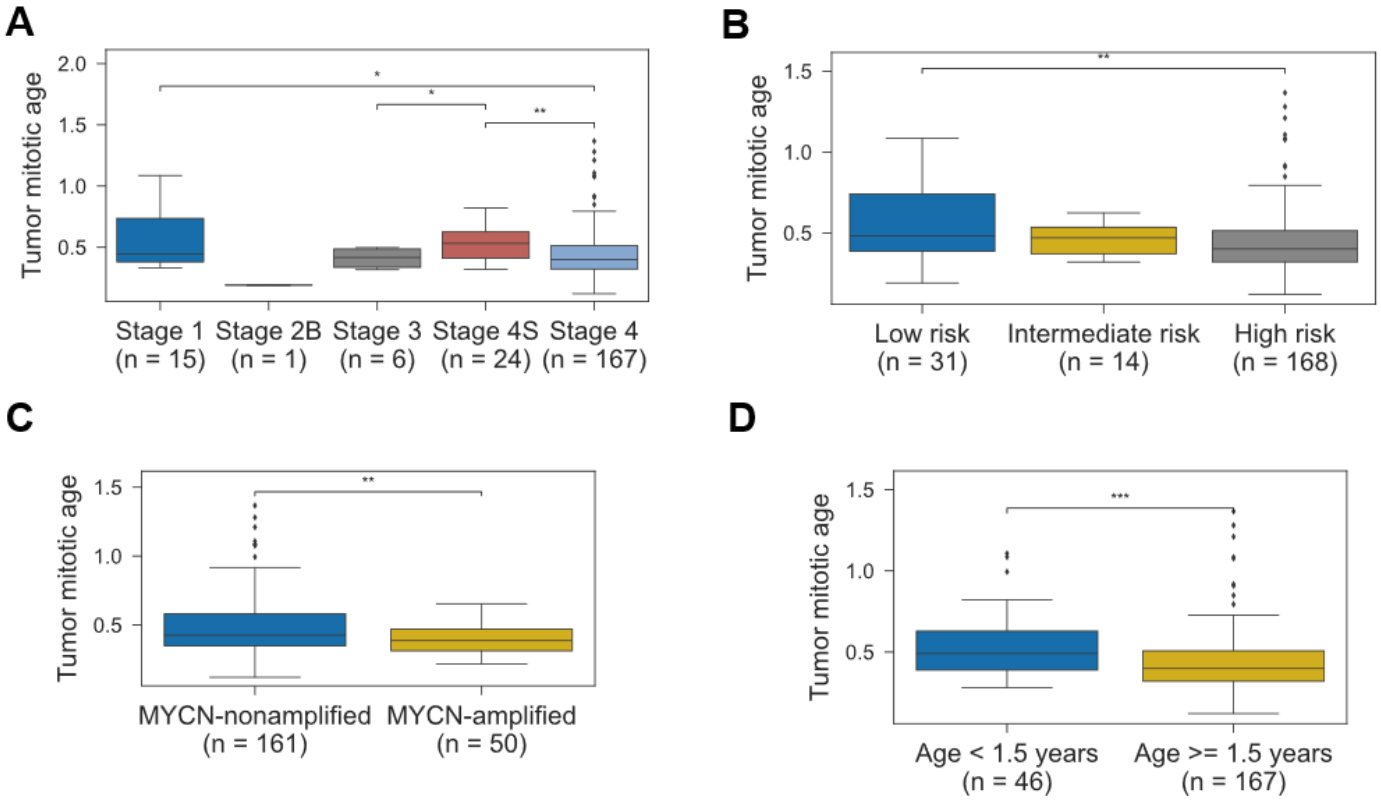

Figure 3. Tumor age vs. clinicopathological variables. The distribution of tumor age values among TARGET NBs, by **(A)** tumor stage; **(B)** risk category; **(C)** MYCN amplification status**;** and **(D)** patient age stratified at 1.5 years. Pairwise comparisons of medians were performed using a two-sided Wilcoxon rank-sum test (*P< 0.05, **P< 0.01, ***P< 0.001). Similar findings were observed with 105 NB samples from GSE73515 (12) (Supplemental Fig. S3).

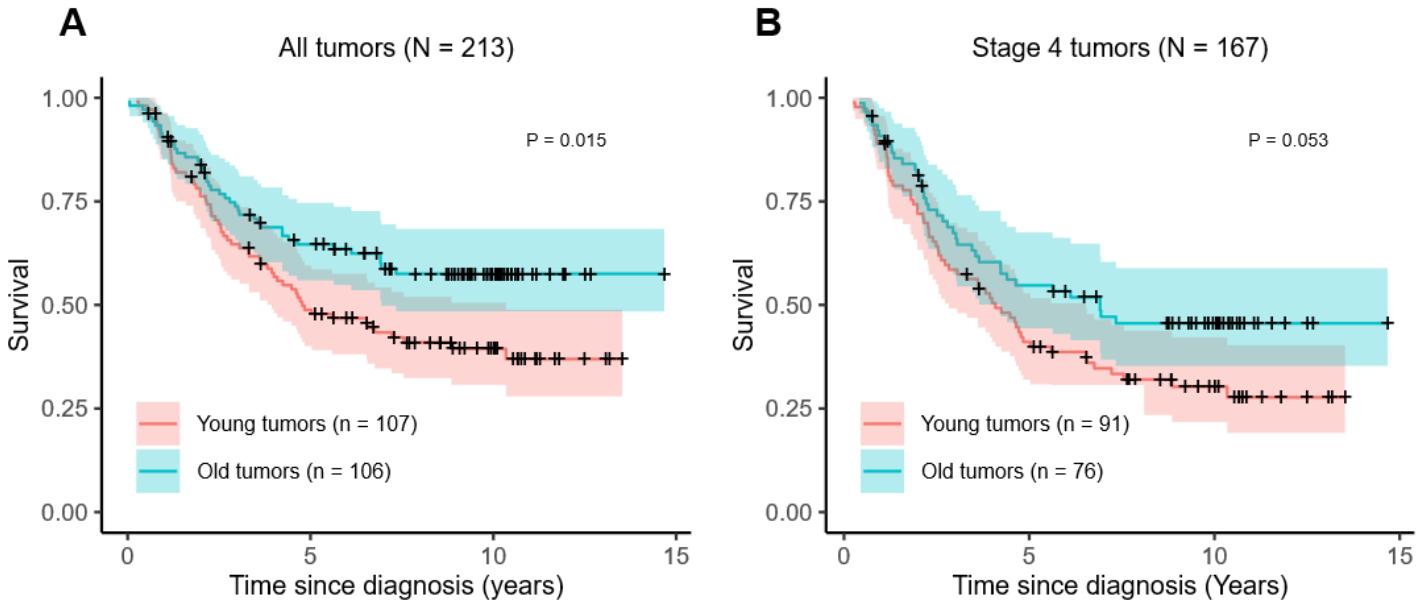

Figure 4. Tumor age vs. survival. Kaplan-Meier survival curves for overall survival, comparing the mitotically youngest 50% and oldest 50% of all tumors as determined by tumor mitotic age. Results are shown in **(A)** all tumors; **(B)** stage 4 tumors. Survival was compared between old and young tumors using the log-rank test.

264 **REFERENCES**

265

266 1. WALTER SD, DAY NE. ESTIMATION OF THE DURATION OF A PRE-CLINICAL DISEASE STATE USING SCREENING
267 DATA. American Journal of Epidemiology. 1983;118(6):865-86. doi: 10.1093/oxfordjournals.aje.a113705.

268 2. Duffy SW, Nagtegaal ID, Wallis M, Cafferty FH, Houssami N, Warwick J, et al. Correcting for Lead Time and
269 Length Bias in Estimating the Effect of Screen Detection on Cancer Survival. American Journal of Epidemiology.
270 2008;168(1):98-104. doi: 10.1093/aje/kwn120.

271 3. Srivastava S, Koay EJ, Borowsky AD, De Marzo AM, Ghosh S, Wagner PD, et al. Cancer overdiagnosis: a biological
272 challenge and clinical dilemma. Nature Reviews Cancer. 2019;19(6):349-58. doi: 10.1038/s41568-019-0142-8.

273 4. Woods WG. Screening for Neuroblastoma Using Urinary Catecholamines: The End of the Story. JNCI Cancer
274 Spectrum. 2021;5(4). doi: 10.1093/jncics/pkab042.

275 5. Brodeur GM. Spontaneous regression of neuroblastoma. Cell and Tissue Research. 2018;372(2):277-86. doi:
276 10.1007/s00441-017-2761-2.

277 6. Matthay KK, Maris JM, Schleiermacher G, Nakagawara A, Mackall CL, Diller L, et al. Neuroblastoma. Nature
278 reviews Disease primers. 2016;2:16078.

279 7. Woods WG, Gao R-N, Shuster JJ, Robison LL, Bernstein M, Weitzman S, et al. Screening of infants and mortality
280 due to neuroblastoma. New England Journal of Medicine. 2002;346(14):1041-6.

281 8. Schilling FH, Spix C, Berthold F, Erttmann R, Fehse N, Hero B, et al. Neuroblastoma screening at one year of age.
282 New England Journal of Medicine. 2002;346(14):1047-53.

283 9. Berthold F, Spix C, Erttmann R, Hero B, Michaelis J, Treuner J, et al. Neuroblastoma Screening at 1 Year of Age:
284 The Final Results of a Controlled Trial. JNCI Cancer Spectrum. 2021;5(4). doi: 10.1093/jncics/pkab041.

285 10. Acharya S, Jayabose S, Kogan SJ, Tugal O, Beneck D, Leslie D, et al. Prenatally diagnosed neuroblastoma. Cancer.
286 1997;80(2):304-10. doi: https://doi.org/10.1002/(SICI)1097-0142(19970715)80:2<304::AID-CNCR19>3.0.CO;2-Y.

287 11. Marshall GM, Carter DR, Cheung BB, Liu T, Mateos MK, Meyerowitz JG, et al. The prenatal origins of cancer.
288 Nature Reviews Cancer. 2014;14(4):277-89. doi: 10.1038/nrc3679.

289 12. Körber V, Stainczyk SA, Kurilov R, Henrich K-O, Hero B, Brors B, et al. Neuroblastoma arises in early fetal
290 development and its evolutionary duration predicts outcome. Nature Genetics. 2023;55(4):619-30. doi: 10.1038/s41588-
291 023-01332-y.

292 13. Caravagna G. Mathematical modeling of neuroblastoma associates evolutionary patterns with outcomes. Nature
293 Genetics. 2023;55(4):530-1. doi: 10.1038/s41588-023-01358-2.

294 14. Gabbutt C, Schenck RO, Weisenberger DJ, Kimberley C, Berner A, Household J, et al. Fluctuating methylation
295 clocks for cell lineage tracing at high temporal resolution in human tissues. Nature Biotechnology. 2022;40(5):720-30.
296 doi: 10.1038/s41587-021-01109-w.

297 15. Monyak DL, Holloway ST, Gumbert GJ, Grimm LJ, Hwang ES, Marks JR, et al. Mapping the temporal landscape of
298 breast cancer using epigenetic entropy. Communications Biology. 2025;8(1):1477. doi: 10.1038/s42003-025-08867-2.

299 16. Institute NC. TARGET: Therapeutically Applicable Research to Generate Effective Treatments2024. Available
300 from: https://www.cancer.gov/ccg/research/genome-sequencing/target.

301 17. Henrich K-O, Bender S, Saadati M, Dreidax D, Gartlgruber M, Shao C, et al. Integrative Genome-Scale Analysis
302 Identifies Epigenetic Mechanisms of Transcriptional Deregulation in Unfavorable Neuroblastomas. Cancer Research.
303 2016;76(18):5523-37. doi: 10.1158/0008-5472.Can-15-2507.

304 18. Hannum G, Guinney J, Zhao L, Zhang L, Hughes G, Sadda S, et al. Genome-wide Methylation Profiles Reveal
305 Quantitative Views of Human Aging Rates. Molecular Cell. 2013;49(2):359-67. doi: 10.1016/j.molcel.2012.10.016.

306 19. Horvath S. DNA methylation age of human tissues and cell types. Genome Biology. 2013;14(10):3156. doi:
307 10.1186/gb-2013-14-10-r115.

308 20. Youn A, Wang S. The MiAge Calculator: a DNA methylation-based mitotic age calculator of human tissue types.
309 Epigenetics. 2018;13(2):192-206. doi: 10.1080/15592294.2017.1389361.

310 21. Zhou W, Dinh HQ, Ramjan Z, Weisenberger DJ, Nicolet CM, Shen H, et al. DNA methylation loss in late-replicating
311 domains is linked to mitotic cell division. Nature Genetics. 2018;50(4):591-602. doi: 10.1038/s41588-018-0073-4.

312 22. Bell CG, Lowe R, Adams PD, Baccarelli AA, Beck S, Bell JT, et al. DNA methylation aging clocks: challenges and
313 recommendations. Genome Biology. 2019;20(1):249. doi: 10.1186/s13059-019-1824-y.

314 23. Teschendorff AE, Horvath S. Epigenetic ageing clocks: statistical methods and emerging computational
315 challenges. Nature Reviews Genetics. 2025;26(5):350-68. doi: 10.1038/s41576-024-00807-w.

316 24. Subramanian A, Tamayo P, Mootha VK, Mukherjee S, Ebert BL, Gillette MA, et al. Gene set enrichment analysis:
317 A knowledge-based approach for interpreting genome-wide expression profiles. Proceedings of the National Academy of
318 Sciences. 2005;102(43):15545-50. doi: doi:10.1073/pnas.0506580102.

319